

The hollow porous sphere cell carrier for the dynamic 3D cell culture

Weidong Gao^{1,3}, Lan Xiao^{1,3}, Jiaqiu Wang², Yuqing Mu^{1,3}, Jayanti Mendhi¹, Wendong Gao^{1,3}, Zhiyong Li², Prasad Yarlagadda², Chengtie Wu^{3,4}, Yin Xiao^{1,3,5}*

¹Centre for Biomedical Technologies, Queensland University of Technology, 60 Musk Avenue, Kelvin Grove, Brisbane, QLD 4059, Australia

²School of Mechanical, Medical and Process Engineering, Queensland University of Technology, 2 George St, Brisbane City QLD 4000, Australia

³The Australia-China Centre for Tissue Engineering and Regenerative Medicine (ACCTERM), 60 Musk Avenue, Kelvin Grove, Brisbane, QLD 4059, Australia

⁴Shanghai Institute of Ceramics, Chinese Academy of Sciences, 1295 Ding-Xi Road, Shanghai 200050, China

⁵School of Medicine and Dentistry, Griffith University, Gold Coast, QLD 4222, Australia

w6.gao@qut.edu.au, +61-0421602838

l5.xiao@qut.edu.au, +61-7-31386245

jiaqiu.wang@qut.edu.au, +61-0422388739

yuqing.mu@hdr.qut.edu.au, +61-7-31386256

jayantiarun.mendhi@hdr.qut.edu.au, +61-7-31386365

w24.gao@qut.edu.au, +61-0405846678

zhiyong.li@qut.edu.au, +61-7-3138 5112

y.prasad@qut.edu.au, +61-7-3138 5167

chengtiewu@mail.sic.ac.cn, +86-21-52412990

***Corresponding Author**

Professor Yin Xiao Tel: +61-7-31386240; Fax: +61-7-31386030

Email: yin.xiao@griffith.edu.au" yin.xiao@griffith.edu.au;

<https://experts.griffith.edu.au/6826-yin-xiao>

Director of Australia-China Centre for Tissue Engineering and Regenerative Medicine
(ACCTERM). <https://research.qut.edu.au/accterm/>

Abstract: Large-scale mammalian cell culture is essential in cell therapy, vaccine production, and the manufacturing of therapeutic protein drugs. Due to the adherent growth characteristic of most mammalian cell types, the combination of cell carrier and bioreactor is a common choice in large-scale mammalian cell culture. Current cell carriers developed by either polymer crosslinking, lithography, or emulsion drops are unable to obtain a structure with uniform porous structure and porous interior design, which results in an inhomogeneous culture condition for cells and therefore can not ensure an optimal dynamic culture condition for cell proliferation, matrix production, and cell differentiation. In addition, the fluidic shear stress (a standard mechanical stimulation in bioreactor culture) and inner-carrier velocity (to ensure nutrient transport and waste exchange), which influence cell viability and growth, are not well-controlled/analyzed due to an irregular porous structure with these traditionally synthesized cell carriers. To solve these problems, we designed 4 types of hollow porous spheres (HPS, 1.0 cm diameter) with different porous structures. To investigate the impacts of porous structure on surface shear stress and inner velocity, computational fluid dynamics (CFD) simulations were conducted to analyze the liquid flow behavior in HPSs, based on which an optimal structure with minimal surface shear stress and best inner velocity was obtained and fabricated using Fused deposition modelling (FDM) 3D printing technology. Inspired by the industrial large-scale culture system, a novel 3D dynamic culture system was then established using HPSs to seed the cells, which were then placed in a mini bioreactor on a tube roller. CFD analysis showed that under 0.1 m/s water flow, the shear stress at most surface areas from four HPSs was lower than 20 dynes/cm², which suggests the HPSs should provide protection against physical stress to the cells living on the scaffold surface. A dynamic cell seeding was developed and refined using the 3D culture system, which increased the 32% seeding efficiency of MC3T3 cells compared to the traditional static cell seeding method. The cell proliferation analysis demonstrated that HPSs could speed up cell growth in dynamic cell culture. The HPS with a honeycomb-like structure showed the highest inner pore velocity (CFD analysis) and achieved the fastest cell proliferation and the highest cell viability. Overall, our study, for the first time, developed a 3D printed HPS cell culture device with a uniform porous structure, which can effectively facilitate cell

adhesion and proliferation in the dynamic cultural environment, thereby could be considered an ideal carrier candidate.

KEYWORDS: 3D printing, 3D cell culture, Dynamic cell culture, Computational fluid dynamics simulation, cellular viability, porous hollow spheres, cell carrier, bioreactor.

Impact Statement

Cell carrier is critical for anchorage-dependent mammalian cells living in a dynamic bioreactor. This study developed the hollow porous spheres (HPS) as a potential cell carrier to facilitate anchorage-dependent mammalian cell growth in a dynamic culture system. Combining the computational simulation, the study result demonstrates that the velocity of the culture medium inside these cell carriers can improve the efficiency of nutrition and oxygen exchange for cell growth in HPS, which is essential for cell metabolism and viability. This study established a method of 3D printed cell carrier for cell growth in a dynamic bioreactor, which could potentially be used as a 3D dynamic cell culture approach for future biomedical research.

Introduction

The cell culture technique is one of the most common tools in biomedical research, which helps people to study cellular behavior and mechanisms in various diseases such as Diabetes, Heart disease, cancer, Alzheimer's disease, etc. Since Harrison, a pioneer in cell culture, developed an approach to culture nerve fiber cells *in vitro* in 1907, most cell studies were conducted in a 2D static environment using the cell flask, disk, and plates^{1,2}. However, the cell lives in a 3D and dynamic environment *in vivo*, and its behaviour is significantly different from the cell in 2D static flask culture, suggesting the importance of applying a 3D cell culture system in biomedical research and the pharmaceutical industry^{3,4}. Meanwhile, previous research has demonstrated that mechanical force derived from the dynamic environment could also play an essential role in cellular behaviours such as proliferation, migration, differentiation, metabolism, and apoptosis⁵⁻¹¹. Hence, the cell culture system combines 3D with the dynamic condition to simulate an environment more analogical to the *in vivo* condition for cell culture, thereby facilitating biomedical research and drug testing for the pharmaceutical industry.

For 3D adherent cell culture, scaffolds are frequently used to allow cell growth in 3 dimensions.¹²⁻¹⁴ However, simulating a dynamic fluidic condition with these scaffolds remains challenging. In the pharmaceutical industry, a common approach for large-scale mammalian cell culture is to use a bioreactor due to the capacities of high output in cell numbers and cost-effective labour cost,^{15,16} which depends on sphere-shaped cell carriers to seed cells. Such an approach can ensure both 3D and dynamic fluidic conditions for cells. It is considered to modify this system into a smaller laboratory device for biomedical research.

Despite the size, developing better cell carriers for cell culture in the bioreactor is critical. Currently, several types of cell carriers have been used, such as dextran-based Cytodex 1 (GE Healthcare) positively charged carriers, dextran-based Cytodex 3 (GE Healthcare) ECM (Extracellular matrix)-coated carriers, polystyrene-based HyQ-spheres (Thermo Scientific) non-charged carriers.¹⁷ Most of these cell carriers are a solid sphere structure, which could result in shear stress and collision damage for cells growing on the carrier surface in the dynamic cell culture system. It is known that adherent cells are sensitive to shear

stress and physical collisions. It has been found that physical stimulus generated in stirring-bioreactor results in cell growth reduction, detachment, and death.^{18,19} Moreover, the dynamic force would induce mechanotransduction to the cultured cells, which will influence cell behavior or even determine cell fate.²⁰⁻²² It is, therefore, necessary to develop an advanced cell carrier that can protect cells from extreme shear force stress in the bioreactor.

A cell carrier with a defined porous structure will provide optimized cell growth and protein production environment. A microporous carrier has been developed to increase the surface areas and avoid collision damage.^{23,24} However, the drawbacks of current microporous carriers are irregular pore size and structure and inhomogeneity of pore size. Besides, the unconnected pore structure makes nutrient exchange and removal of cell waste difficult. These limitations are mainly due to the traditional manufacturing methods. Thereby, it is necessary to develop advanced microporous carriers with the ideal structure in a precisely controlled way, and a procedure could be achieved via 3D printing technology.

3D printing technology can manufacture objects layer by layer, which includes Fused Deposition Modelling (FDM), Digital Light Processing (DLP), Selective Laser Melting (SLM), Stereolithography (SLA), Laminated Object Manufacturing (LOM), Selective Laser Sintering (SLS), and Digital Beam Melting (EBM).¹³ These technologies have been used to produce products with sizes ranging from millimeters to nanometers. 3D printing is capable of fabricating complex structures precisely according to the design. Moreover, various types of material (e.g., polymer, metal, and ceramics) can be chosen to fabricate 3D-printed products based on their application.¹⁴ Polymers, such as Polylactic acid (PLA), Polycaprolactone, Polystyrene and natural gelatin methacrylate, are widely used to fabricate scaffolds for cell adhesion and growth for tissue engineering study due to the characteristic of suitable mechanical strength to maintain a 3D structure under certain external stress.²⁵ Especially, some synthetic polymers have been approved by Food and Drug Administration (FDA, USA) for clinical use, which are highly biocompatible and thereby beneficial for cell growth.²⁶ Thus, a 3D printed polymer scaffold could be developed with the pre-designed structure to fulfil cell growth and proliferation in a

dynamic suspension culture environment. Furthermore, the Langmuir–Blodgett (LB) technique has been developed and used to precisely control the coverage of the deposited biomaterial on the material surface, which is considered a different advanced approach for precise surface modification.

In this study, we firstly designed a novel 3D dynamic culture system using a sphere-shaped scaffold, mini bioreactor and tube roller. Then, to develop an ideal scaffold, four types of hollow porous spheres (HPS) were designed by Rhino software with different pore structures to minimize collision damage and shear stress, which were then accordingly fabricated *via* 3D printing. To examine whether the pre-designed structure could ensure sufficient carrier inside-outside nutrition/waste exchange, a computational model based on the ANSYS Workbench platform was established to analyze the fluid property of these four HPSs. A dynamic cell seeding method was developed and optimized to achieve a high seeding efficiency with HPS. Finally, we evaluated the effects of static/dynamic culture methods and different HPS structures on cell growth speed and viability to find the most suitable carrier for future application in the bioreactor-based cell dynamic culture system. Based on our data, the novel 3D dynamic cell culture system has been established, with a refined HPS structure that can be applied in not only the current culture system but also the large-scale industrial cell culture.

Method

In this study, 4 different hollow porous spheres (HPS) with 1.0 cm diameter were fabricated by fused deposition modelling (FDM) 3D printer, and the surface was modified by plasma treatment to facilitate anchorage-dependent mammalian cell growth in a dynamic culture system. A dynamic cell seeding method has been established to improve the cell seeding efficiency on the HPS 3D cell carrier and has been tested by PicoGreen assay showing the total DNA amounts of cells on HPS and AlamarBlue assay showing cells viability on HPS after seeding. In addition, computational fluid dynamics (CFD) was performed to test the flow behaviour of 4 types of HPSs and the osteoblast precursor cell line MC3T3 was used in testing cell proliferation profiles of 4 types of HPSs in a dynamic culture environment.

Experiment

Design of HPS 3D geometric models

The models for HPS were constructed by the solid modelling program (McNeel R, & others. (2010). Rhinoceros 3D, Version 6.0. Robert McNeel & Associates, Seattle, WA). Firstly, a 1.0 cm-diameter sphere with a 0.4 cm-diameter sphere-shaped inner hollow was created. Then Rhinoceros transform tool was used to create the different porous shapes with various aperture sizes. Finally, models were saved as STereoLithography (STL) files for 3D fabrication.

Fluid property analysis of HPS structures with ANSYS Workbench platform

The computational fluid dynamics (CFD) was performed on the commercial CFD software Fluent at ANSYS Workbench platform (ANSYS 19.0, ANSYS Inc., Canonsburg, PA, USA). To assess the flow behavior passing through different HPS structures, HPS models were placed into a cylinder fluid domain (100.0 mm in diameter and 2000.0 mm in length). The whole fluid domain was relatively larger than HPS, which was the region of interest (ROI), to guarantee the flow reached the HPS structural area was fully developed and away from the boundary. To save computational consumption, multi-level mesh size was applied to the fluid domain, where only the HPS area was given the finest mesh. The curvature mesh size function was applied to the fluid domain. Furthermore, four levels of concentric sphere body sizing controls were given to the HPS area (Table 1), and 5 and 10 inflation layers were applied to the boundary of cylinder fluid area and HPS area, respectively. Water liquid (density of 998.2 kg/m^3 and viscosity of $100.3 \times 10^{-5} \text{ kg/m}\cdot\text{s}$) was used in this study. Steady and laminar 0.1 m/s velocity inlet and 0 Pa constant pressure outlet were given as boundary conditions. A maximum of 5000 iterations were allowed for calculation.

HPS fabrication via FDM 3D printing

A Wombat 3D printer (Keysborough, VIC) was used for HPS with 1 cm diameter printing. PLA filaments with 1.75 mm diameter were purchased from Bilby 3D (Brisbane, QLD). 0.4 mm-diameter Brass nozzle was used. The nozzle temperature was set at $210 \text{ }^\circ\text{C}$ and the

printing bed temperature was set at 70 °C to preclude the printed material from warping. Multi-scaffold models were placed in one G-cold and printed *via* sequential printing.

Scanning electron microscopy of PCL scaffolds

HPS samples were coated by a benchtop sputtering device (EM SCD005, Leica Microsystems) with an ultrathin (~10 nm) layer of gold and mounted onto aluminium stubs. Samples were visualized using a Jeol 7001F Scanning Electron Microscope (Jeol, Japan).

Surface modification of HPS by plasma treatment

HPSs were treated by plasma to enhance their hydrophilicity surface character and therefore promote cell attachment.^{29,30} Harrick Plasma machine (Harrick Plasma, Expanded Plasma Cleaner PDC-002) was used for the plasma surface modification process, HPSs were placed on the plasma cleaner chamber when it was pumped down to a base pressure of 120–160 mTorr. Then argon and oxygen gas (at a ratio of 3:1) was injected into the chamber using an MKS mass flow (MKS Instruments, Inc., USA), and a radio frequency (RF) power of 10.2 W was applied to initiate the plasma. Samples were exposed to plasma for 10 min. The chamber was then purged with air to open. HPSs were turned upside down and re-treated by plasma. HPSs were then removed from frames and sterilized *via* immersion in 75% ethanol for 1h, followed by air-drying in a biosafety class II cabinet.

Cell seeding and culture on HPS scaffolds

The cell line, MC3T3 (MC3T3-E1 Subclone), was used in this study. MC3T3 cells were maintained in culture medium Dulbecco's Modified Eagle Medium (DMEM; Gibco®, Life Technologies Pty Ltd., Australia) supplemented with 10 % fetal calf serum (FCS; In Vitro Technologies, Australia) and 1 % (50 U/ml and 50 µg/ml, respectively) penicillin/streptomycin (P/S; Gibco®, Life Technologies Pty Ltd., Australia) at 37 °C with 5 % CO₂.

In the current study, static and dynamic cell seeding methods were applied and compared:

For static cell seeding on the carriers, 6 HPSs were put in one 15 ml centrifuge tube. Total cells (2×10^5 /scaffold) were suspended in 10 ml cell culture medium to seed on HPSs in one tube. The tube was placed in the incubator for 10 h. For dynamic cell seeding, total cells (2×10^5 /scaffold) were suspended in 10 ml medium on 6 HPSs in one 15 ml centrifuge tube. The tube was put horizontally on the Tube Roller (Thermo Scientific, Australia). The tube roller was then placed in the incubator and set with different rolling speeds (10 rpm, 20 rpm, 30 rpm and 40 rpm) for 10 h of seeding. For both seeding methods, HPSs were collected, and the seeding efficiency was compared via alamarBlue cell viability assay and PicoGreen assay.

To compare the effects of dynamic and static cell culture on cell proliferation, 60 HPSs seeded with cells were placed in six 50ml Mini Centrifuge Bioreactors with Vent Cap (Corning Inc, Australian). Each mini bioreactor contained 10 HPSs suspended in 30 ml culture medium. For dynamic culture, 3 mini bioreactors were horizontally placed on the Tube Roller with the speed of 10 rpm for dynamic cell culture. Another 3 mini bioreactors were put on the incubator layer for static cell culture. Every 24 h cells on HPS were analyzed with alamarBlue cell viability assay and PicoGreen assay to evaluate cell proliferation from day 1 to day 10.

AlamarBlue cell viability assay and PicoGreen assay

Cell metabolic activity and DNA content were measured by AlamarBlue cell viability assay and PicoGreen assay, respectively, to assess the cell amount on HPS. For alamarBlue assay, a 10% alamarBlue (Thermo Scientific) working solution was pre-prepared. HPS was transferred to a 24 well-plate and 1.5 ml alamarBlue working solution was then added. Empty wells with the working solution at the same amount served as the negative control. The plates were incubated at 37 °C for 2 h, and 300 ul medium from each HPS-well was transferred into 3 wells from a 96-well black plate (100 ul/well). Fluorescence extensity (excitation 544 nm, emission 590 nm) was measured using a plate reader (BMG Omega, BMG LABTECH).

The PicoGreen assay was performed using the PicoGreen assay kit (Invitrogen Ltd., Australia) according to the supplied protocol. Lambda DNA standards were used to generate the standard curve. The cells were harvested from the HPS by treating them with 0.5% trypsin (1.5ml per HPS) at 37 °C for 3 min. The cell suspension was centrifuged for 5 min at 1000 rpm, and the cell pellet was washed twice with PBS (Phosphate-buffered saline). After that, cells were resuspended in 2ml TE buffer, frozen in a -80 °C freezer overnight and thawed at 37 °C. Samples were aliquoted in triplicate into a 96-wells plate (100 ul/well) and incubated with PicoGreen assay reagent, then read with a fluorescence plate reader (BMG Omega, BMG LABTECH; excitation 485 nm, emission 520 nm).

Live/dead staining

Fluorescein diacetate (FDA) is a cell-permeable esterase substrate that measures both enzymatic activity and cell membrane integrity, which is used to detect live cells. Propidium iodide (PI) is a small fluorescent molecule that binds to DNA but cannot passively traverse into cells that possess an intact plasma membrane, which could be used to detect cell death. Thereby, to evaluate cell viability, cell-seeding HPSs were incubated with 2 mg/mL FDA (Sigma-Aldrich) for 15 min and then 20 mg/mL PI (Sigma-Aldrich) for 5 mins at 37°C to stain live and dead cells, respectively. Cells were then observed and imaged by Nikon SMZ25 Stereo Microscope.

Evaluating Cell Death by Flow Cytometry

Flow cytometry was performed to further measure the percentage of dead cells (in total population) on HPS under different culture conditions. Cells were harvested from HPS and treated with 1ug/ml PI at room temperature for 15 min. Cell death (percentage of PI-positive cells in total) was measured by flow cytometry (BD FACSCelesta Flow Cytometer). The cell population size for analysis is 50,000 in this study. Data were collected and analyzed by FACSDiva software.

Statistical Analysis

All statistical analyses were performed using SPSS 13.0 (SPSS Inc., Chicago, IL). Student T-tests were performed for comparison between the two groups. For comparison in multiple

groups, data were subjected to one-way ANOVA followed by the Student–Newman–Keul test at $\alpha = 0.05$. $P < 0.05$ was considered significantly different.

Results and Discussion

Design of a novel 3D dynamic culture system

In the pharmaceuticals industry, a large-scale cell culture system is frequently used, which consists of cell carriers and a rotating bioreactor to keep the carrier spinning inside the bioreactor. Inspired by this system, in the current study, a novel laboratory 3D dynamic culture system has been designed. As shown in Figure 1, hollow porous spheres (HPS) are used to seed the cells and allow for 3D cell culture, which is then placed in a mini bioreactor filled with the culture medium. The mini bioreactor is then placed in a tube roller to keep the HPS rotating, an approach to ensure a dynamic fluidic culture environment for the cells living on HPS. Hence, a novel 3D dynamic cell culture system has been designed.

Computer-aided HPS design

Cell carrier provides an opportunity to culture the anchorage-dependent cell in the dynamic culture environment.^{17,20,23} To solve the drawbacks of solid sphere carriers (e.g., collision damage), porous carriers have been developed using traditional chemical synthetic methods, such as crosslinking, lithography and emulsion drop. These methods, however, are merely possible to accurately control the carrier structure according to the design.

3D printing technology provides a manufacturing method to precisely synthesize an object with a complex structure following the design. So, we used this advanced manufacturing method to produce HPS to conquer the drawback of the traditional manufacturing method. We used Rhino (CAD software) to design the structure of the HPS. The most critical design criteria are considered as the physical protection and permeability due to the certain environment in a dynamic culture system. Previous studies have shown that severe shear force in dynamic culture could result in cell growth reduction, detachment and death.^{19,23} To minimize shear force, we designed four types of HPS with porous and

hollow structures to provide an optimized "shelter"—the covered inside space for cell adhesion and growth. The porous structure could effectively protect the cells from shear stress damage, and the hollow design ensured the culture medium easily goes through the scaffold to offer sufficient material exchange, making it more convenient to harvest cells from the porous surface. As shown in Figure 2a, four HPSs (diameter: 1 cm) with different outer pores were constructed by the Rhinoceros. Each of them contained a hollow core structure (diameter: 0.4 cm) to ensure the medium exchange between the inside and outside of the scaffold (Figure 2b). According to the parameters shown in Figure 2c, HPS1 had the largest outer/inner pore sizes and the smallest volume. HPS4 had the largest surface area and volume.

CFD analysis of HPS

The four 1cm-diameter HPSs with the 0.4 cm-diameter inner hollow structure were designed with different pore sizes and outer structures, two factors considered to cause different fluent behaviour in the dynamic culture environment and, therefore, could result in different cell growth and proliferation. Understanding the fluid dynamics behaviours of the scaffolds, such as surface shear stress and inside velocity, would provide us with information about the advantages/disadvantages of different structures and the evaluation criteria for future carrier design and manufacture. An analysis model was established with ANSYS, which has been widely used to simulate dynamic cell culture physical environment.^{31,32} A cylinder model (100.0 mm in diameter and 2000.0 mm in length) was established, and 4-level sphere body sizing was given to the HPS area to balance the computational load and computational precision (Figure S1). In this model, the different HPSs were put in the centre of the cylinder, and 0.1 m/s water flow was going through HPS, a common physical condition to mimic the environment of the real dynamic cell culture. The surface shear stress and velocity inside the HPS were calculated. Figure 3a shows the colour contours of the magnitude of wall surface shear stress (WSS). In ANSYS analysis procedure, the surface of HPS was divided into multiple 0.01 mm² small square areas. The colour ranged from blue to red and showed the strong to weak shear stress intensity on the small square area. The mean volumetric distribution of WSS (values in logarithm) was shown in Figure 3b. The shear stress at most surface areas from four HPSs

was lower than 20 dynes/cm^2 , which suggests the HPSs should provide protection against physical stress to the cells living on the scaffold surface (Figure 3c), as the surface shear stress higher than 2 Pa (20 dynes/cm^2) has been found to impair cell viability in the dynamic culture environment.^{19,23} Based on the CFD results, the four HPSs should be able to provide protection from shear stress damage to cells.

The inside velocity of HPS determines the material exchange between the HPS inside space and the outside environment. High flow could facilitate nutrition and oxygen to get into the scaffolds and metabolic waste to get out of the scaffold. The low inside-outside exchange has been considered to impair the viability of cells living inside the scaffold,^{33,34} suggesting velocity should be another key parameter for our cell carrier design. To analyze the velocity of 4 HPSs, a surface in the middle of HPS was created in CFD, which was divided into multiple 0.01 mm^2 small square areas. The magnitude of flow velocity through the surface was calculated and shown in Figure 3d. Figure 3e shows the mean volumetric distribution of velocity (values in logarithm). From the scatter plot graph of the inside velocity (Figure 3f), HPS1 showed the highest mean value of velocity, and HPS4 showed the lowest. This result indicates that the liquid (culture medium) would go through the HPS1 faster than the other three, suggesting that it should achieve the most efficient nutrition, oxygen and metabolic waste exchange in the dynamic culture.

HPS fabrication and surface modification

After successful design and analysis, HPSs were then fabricated by using FDM 3D printer. Compared to other 3D printers, the advantages of FDM are as follows. 1) Speed: it only takes 16min at average to fabricate a 1cm-diameter HPS. 2) Accuracy: FDM printer uses the filament that is heated to a melting point and then extracted in layers to create a 3D object. The error during the whole process is within 0.005 inches. 3) Ease procedure: FDM printers can directly fabricate most of the items designed by CAD program. FDM printer also has fewer possible satellite droplet issues, usually caused by some soft material such as collagen or fibrinogen, which cannot hold their shape in the fragmentation process of injecting printing. FDM printing usually uses strong, engineering-grade materials such as ABS (Acrylonitrile butadiene styrene) and PLA (Polylactic acid), which could hold their shape

well and produce continuous filament in the printing process and achieve some complex structure printing. In the meantime, if the hot end of the nozzles is too low, the print material will not melt correctly, which could lead to nozzle clogging. Nowadays, the FDM 3D printing, such as Wombot we used, has a precision temperature control unit that could sophisticatedly control the material melt temperature in the nozzle to assure the flow of printing and avoid nozzle clogging. The four types of HPS were fabricated by Wombot 3D printer (FDM) with a 100-micron layer height to meet the requirement of fine detailed structure. The nozzle temperature, bed temperature and printing speed were set accordingly to the previous studies.^{35,36} Figure 4a showed that 32 HPSs could be fabricated by sequential printing in one batch, which saved time, and labor and thereby could satisfy the huge demand for cell culture. The four different HPSs were printed (1 cm diameter), and the structures were consistent with the designed geometry (Figure 4b). The SEM pictures showed the detailed structures of HPSs, which all had wrinkled surfaces due to the layer-by-layer printing procedure (Figure 4c). These wrinkled surfaces could provide more areas for cell adhesion and growth compared to the smooth surface.

In the current study, the biodegradable aliphatic polymer PLA was chosen as the material to print HPS due to its biocompatible and non-toxic features.^{37,38} PLA is an FDA-approved biodegradable aliphatic polymer that was widely used to fabricate the 3D scaffold.³⁷ However, PLA is a low wettability material that affects cell adhesion and proliferation. To solve this, discharge gas plasma was performed, which has been demonstrated to modify the wetting property of PLA to enhance cell adhesion and proliferation on the PLA surface.³⁹ To determine the wettability of the PLA surface after the discharge of gas plasma, the water contact angle measurement was performed. As shown in Figure S2, the PLA film was printed and treated by the same plasma procedure as HPS. After gas-plasma treatment, the contact angle decreases from 73° to 38°, which indicates that PLA surface wettability should be increased.

Cell seeding on HPS

Cell seeding is the first step in the abundant cultivation of mammalian cells in HPS. To examine whether HPS was suitable for cell culture, successful and efficient cell seeding

should be guaranteed. Static seeding is a standard seeding method in 2D cell culture. However, previous research has found that static seeding is not suitable for 3D scaffolds, while dynamic seeding could enhance seeding efficiency.⁴⁰ Adhesion cell number and uniform cell distribution are considered two indexes of seeding efficiency. We used MC3T3 cell line as a study model to test the seeding efficiency. Figure 5a showed that cells seeded dynamically were distributed more uniformly than static seeding. It could be observed that after static seeding, many cells aggregated in some pores, while other pores had few cells. On the other hand, *via* dynamic seeding, cells are distributed evenly in most pores. This phenomenon should be due to the more uniform cell distribution during dynamic cell seeding, as the suspended cells may take a longer time to attach during dynamic seeding. To quantify the amount of cells adherent to HPS surface, alamarBlue assay and PicoGreen assay were performed. From Figure 5b&c, it could be observed that there were significantly increased cell metabolic activity and DNA amount in the dynamic seeding group, suggesting there should be more cells seeding on HPS with this seeding method, which was consistent with the FDA staining result. These results indicate that the dynamic seeding method can achieve better efficiency, as demonstrated by uniform cell distribution and increased cell number.

The roller speed and seeding time are two factors that would affect the dynamic seeding efficiency. We compared the effects of four different roller speeds and seeding times on the dynamic seeding efficiency. As shown in Figure 5d&e, high roller speed at 40 rpm would decrease the number of cells seeding on HPS, as indicated by decreased cell metabolic activity and DNA amount. Moderate speeds such as 10 rpm and 20 rpm resulted in a similar seeding efficiency. The cell amount was monitored for up to 10 h after seeding to optimize the seeding efficiency. It could be observed that the cell amount increased from 2 h to 6 h after seeding, while after that, no obvious change could be observed. This suggests seeding duration should be no less than 6 h for both static and dynamic seeding methods (Figure 5f, g). Some cells that remained in the medium were observed under a microscope after 6 h' of seeding (data not shown), indicating a cellular precipitation effect even using the dynamic seeding method. We also compared the seeding efficiency of 4 different HPSs with the optimized dynamic seeding method (roller speed: 10 rpm, seeding

duration: 8 h) to find whether the structure difference would affect seeding efficiency. The FDA staining result indicates that the seeding efficiency was similar on 4 different structures (Figure S3a), which showed even cell distribution on the scaffold and identical cell amounts, as tested by PicoGreen assay and alamarBlue assay (Figure S3b).

The effects of static and dynamic cell culture on cell proliferation in HPS

The different cell culture methods would affect cell growth by changing the mechanical and chemical features of the cell-living environment.^{41,42} For cells on the scaffold, a previous study has shown that the dynamic culture method would favor cell growth, as it could provide more efficient material exchange between the inside and outside of the scaffold; besides, this liquid exchange could exhibit mechanic stimulation for cell growth.⁴³ In the current study, the cell growth curves showed that for HPSs in dynamic culture, the cell took less time to reach the stationary phase than in the static culture (Figure 6a). Figure 6b&c showed that cells grew faster and took less time to double the cell number in all four different HPSs in the dynamic culture system as compared to the static one. Those results implied that the shear stress on HPS would not cause an obvious negative impact on cell growth, which was consistent with our computational simulation outcome—that all HPS structures should provide efficiency protection against the physical shear stress.

The effect of HPS structure on cell proliferation in a dynamic culture system

As the CFD analysis results showed the velocity difference among the 4 types of HPS, we wondered whether HPS structure would affect cell growth in a dynamic culture. Thus, the growth curves of cells cultured on 4 HPSs were compared (dynamic culture at a roller speed of 10 rpm). The HPS1 took the least time to reach the stationary phase and HPS4 was the slowest one to reach the stationary phase (Figure 6a). Figure 6b&c showed that HPS1 achieved the fastest cell proliferation and took the least time to double the cell number. These results were consistent with the analysis of the inside velocity of HPS. This indicates that the inside-outside material exchange is an important factor for cell growth on HPS. The structure of HPS1 provided the highest material exchange ratio, which could be the reason for the fastest cell growth as compared to the other 3 HPSs.

To evaluate cell viability, cells growing on HPS were analyzed with live/death staining and flow cytometry to detect the portion of dead (PI⁺) cells. Figure 7d&e showed that HPS 4 had the highest percentage of dead cells. The FDA/PI fluorescence staining showed consistent results that the red signal (PI-positive, dead cell) was the lowest in HPS1 and the highest in HPS4. This indicates that the inner velocity inside not only determines the cell growth speed but also affects cell viability when reaching high confluence.

Conclusion

In this study, we developed a novel cell carrier-HPS by FDM 3D printing technology for abundant cultivation of mammalian cells in a dynamic culture system. All HPSs showed a low intensity of surface shear stress. However, HPS1 showed the highest inside velocity, indicating the most efficient material change in HPS1. HPS1 also achieved the fastest cell proliferation with the highest cell viability, which was in accordance with its highest inside velocity, suggesting that inside velocity should be a key index in future cell carrier design. Our 3D printed cell carrier thereby could act as an advanced carrier, which can be applied in large-scale cell culture in the biopharmaceutical industry. Our established strategy to design a cell carrier with a porous structure and suitable inside velocity *via* CFD-aided simulation, and to use 3D printing as the carrier manufacturing method, can guide the design and fabrication of high-throughput cellular bioreactors in the future. Moreover, based on this carrier, we provide a novel 3D dynamic culture system by combining HPS, a small bioreactor and a tube roller, which can be further applied in future biomedical research.

AUTHOR INFORMATION

Corresponding Author

*Yin Xiao, School of Mechanical, Medical and Process Engineering, 60 Musk Avenue, Kelvin Grove, Brisbane, QLD 4059, Australia.; Email: yin.xiao@griffith.edu.au

Authors' Contribution

Conceptualization, Weidong Gao; methodology, Weidong Gao., Lan Xiao., Jiaqiu Wang., Yuqing Mu; formal analysis, Weidong Gao; data curation, Weidong Gao and Jayanti

Mendhi; Writing-original draft preparation, Weidong Gao and Lan Xiao; Writing-review and editing, Yin Xiao., Zhiyong Li., Wendong Gao., Prasad Yarlagadda., Chengtie Wu; project administration, Weidong gao; funding acquisition, Yin Xiao. All authors have read and agreed to the published version of the article.

Notes

The authors declare no competing financial interest.

ACKNOWLEDGEMENT

This project is supported by Australia Research Council Industrial Transformation Training Centre in Additive Biomanufacturing (IC160100026) and funding for JRC in functional biomaterials from the Queensland Government Department of Environment and Science. We thank the staff at the Queensland University of Technology (QUT) Mechanical School for Computational Fluid Dynamics Simulation and technical support.

References

1. Greiner AM, Richter B and Bastmeyer M. Micro-Engineered 3D Scaffolds for Cell Culture Studies. *Macromol Biosci* 2012;12(10):1301-1314; doi: 10.1002/mabi.201200132.
2. Souza AG and C Ferreira IC. Advances in Cell Culture: More than a Century after Cultivating Cells. *J Biotechnol Biomater* 2016;6(2):221; doi: 10.4172/2155-952x.1000221.
3. Edmondson R, Broglie JJ, Adcock AF, et al. Three-Dimensional Cell Culture Systems and Their Applications in Drug Discovery and Cell-Based Biosensors. *Assay Drug Dev Technol* 2014; 12(4):207-18;doi: 10.1089/adt.2014.573.
4. Shamir ER and Ewald AJ. Three-Dimensional Organotypic Culture: Experimental Models of Mammalian Biology and Disease. *Nat Rev Mol Cell Biol* 2014;15:647-664; doi: 10.1038/nrm3873.
5. Noesch H. Mechanical Forces Direct Stem Cell Behaviour in Development and Regeneration. *System* 1967;18(12):30–38; doi: 10.1016/j.bone.2016.06.013.The.
6. Gmünder FK, Nordau CG, Tschopp A, et al. Dynamic Cell Culture System: A New Cell Cultivation Instrument for Biological Experiments in Space. *J Biotechnol* 1988;7(3):217–227; doi: 10.1016/0168-1656(88)90053-3.
7. Bale SS and Borenstein JT. Microfluidic Cell Culture Platforms to Capture Hepatic Physiology and Complex Cellular Interactions. *Drug Metab Dispos* 2018;46(11):1638–1646; doi: 10.1124/dmd.118.083055.
8. Coluccio ML, Perozziello G, Malara N, et al. Microfluidic Platforms for Cell Cultures and Investigations. *Microelectron Eng* 2019;208(June 2018):14–28; doi: 10.1016/j.mee.2019.01.004.
9. Hansmann J, Egger D and Kasper C. Advanced Dynamic Cell and Tissue Culture. *Bioengineering* 2018;5(3):5–7; doi: 10.3390/bioengineering5030065.

10. Quinlan AM, Sierad LN, Capulli AK, et al. Combining Dynamic Stretch and Tunable Stiffness to Probe Cell Mechanobiology in Vitro. *PLoS One* 2011;6(8): e23272;doi: 10.1371/journal.pone.0023272.
11. Alrezk R, Hannah-Shmouni F, and Stratakis CA. Effect of Dynamic Culture and Periodic Compression on Human Mesenchymal Stem Cell Proliferation and Chondrogenesis. *Physiol Behav* 2017;176(12):139–148; doi: 10.1016/j.physbeh.2017.03.040.
12. Yuan H, Xing K and Hsu H-Y. Trinity of Three-Dimensional (3D) Scaffold, Vibration, and 3D Printing on Cell Culture Application: A Systematic Review and Indicating Future Direction. *Bioengineering* 2018;5(3):57; doi: 10.3390/bioengineering5030057.
13. Do AV, Khorsand B, Geary SM, et al. 3D Printing of Scaffolds for Tissue Regeneration Applications. *Adv Healthc Mater* 2015;4(12):1742–1762; doi: 10.1002/adhm.201500168.
14. An J, Teoh JEM, Suntornnond R, et al. Design and 3D Printing of Scaffolds and Tissues. *Engineering* 2015;1(2):261–268; doi: 10.15302/j-eng-2015061.
15. Eaker S, Abraham E, Allickson J, et al. Bioreactors for Cell Therapies: Current Status and Future Advances. *Cytotherapy* 2017;19(1):9–18; doi: 10.1016/j.jcyt.2016.09.011.
16. Merten OW. Advances in Cell Culture: Anchorage Dependence. *Philos Trans R Soc B Biol Sci* 2015;370(1661): 20140040; doi: 10.1098/rstb.2014.0040.
17. Martin Y, Eldardiri M, Lawrence-Watt DJ, et al. Microcarriers and Their Potential in Tissue Regeneration. *Tissue Eng - Part B Rev* 2011;17(1):71–80; doi: 10.1089/ten.teb.2010.0559.
18. Wu S. Influence of Hydrodynamic Shear Stress on Microcarrier-Attached Cell Growth : Cell Line Dependency and Surfactant Protection. *Bioprocess Eng* 1999;21:201–206; doi: 10.1007/s004490050663.

19. Hua J, Erickson LE, Yiin TY, et al. A Review of the Effects of Shear and Interfacial Phenomena on Cell Viability. *Crit Rev Biotechnol* 1993;13(4):305–328; doi: 10.3109/07388559309075700.
20. Leung HW, Chen A, Choo ABH, et al. Agitation Can Induce Differentiation of Human Pluripotent Stem Cells in Microcarrier Cultures. *Tissue Eng - Part C Methods* 2011;17(2):165–172; doi: 10.1089/ten.tec.2010.0320.
21. Burridge K, Monaghan-Benson E and Graham DM. Mechanotransduction: From the Cell Surface to the Nucleus via RhoA. *Philos Trans R Soc B Biol Sci* 2019;374(1779): 20180229; doi: 10.1098/rstb.2018.0229.
22. Tai LK, Okuda M, Abe J ichi, et al. Fluid Shear Stress Activates Proline-Rich Tyrosine Kinase via Reactive Oxygen Species-Dependent Pathway. *Arterioscler Thromb Vasc Biol* 2002;22(11):1790–1796; doi: 10.1161/01.ATV.0000034475.40227.40.
23. Nilsson K. Microcarrier Cell Culture. *Biotechnol Genet Eng Rev* 1988;6(1):403–439; doi: 10.1080/02648725.1988.10647854.
24. Nilsson K, Buzsaky F, and Mosbach K. Growth of Anchorage-Dependent Cells on Macroporous Microcarriers. *Nat Biotechnol* 1986;4:719–725; <https://doi.org/10.1038/nbt1186-989>.
25. Dawood A, Marti BM, Sauret-Jackson V, et al. 3D Printing in Dentistry. *Br Dent J* 2015;219(11):521–529; doi: 10.1038/sj.bdj.2015.914.
26. Guvendiren M, Molde J, Soares RMD, et al. Designing Biomaterials for 3D Printing. *ACS Biomater Sci Eng* 2016;2(10):1679–1693; doi: 10.1021/acsbiomaterials.6b00121.
27. Marcuello C, Foulon L, Chabbert B, et al. Langmuir-Blodgett Procedure to Precisely Control the Coverage of Functionalized AFM Cantilevers for SMFS Measurements: Application with Cellulose Nanocrystals. *Langmuir* 2018;34(32):9376–9386; doi: 10.1021/acs.langmuir.8b01892.

28. Fernández L, Reviglio AL, Heredia DA, et al. Langmuir-Blodgett Monolayers Holding a Wound Healing Active Compound and Its Effect in Cell Culture. A Model for the Study of Surface Mediated Drug Delivery Systems. *Heliyon* 2021;7(3): e06436; doi: 10.1016/j.heliyon.2021.e06436.
29. Wu C, Fan W, Zhou Y, et al. 3D-Printing of Highly Uniform CaSiO₃ Ceramic Scaffolds: Preparation, Characterization and in Vivo Osteogenesis. *J Mater Chem* 2012;22(24):12288–12295; doi: 10.1039/c2jm30566f.
30. Fomby P, Cherlin AJ, Hadjizadeh A, et al. Endothelial Cell Behaviour on Gas-Plasma-Treated PLA Surfaces: The Roles of Surface Chemistry and Roughness. *Ann Am Thorac Soc* 2010;12(3):181–204; doi: 10.1002/term.
31. Huang M, Fan S, Xing W, et al. Microfluidic Cell Culture System Studies and Computational Fluid Dynamics. *Math Comput Model* 2010;52(11–12):2036–2042; doi: 10.1016/j.mcm.2010.01.024.
32. Galbusera F, Cioffi M, Raimondi MT, et al. Computational Modeling of Combined Cell Population Dynamics and Oxygen Transport in Engineered Tissue Subject to Interstitial Perfusion. *Comput Methods Biomech Biomed Engin* 2007;10(4):279–287; doi: 10.1080/10255840701318404.
33. Bergemann C, Elter P, Lange R, et al. Cellular Nutrition in Complex Three-Dimensional Scaffolds: A Comparison between Experiments and Computer Simulations. *Int J Biomater* 2015;2015: 584362; doi: 10.1155/2015/584362.
34. Piard CM, Chen Y and Fisher JP. Cell-Laden 3D Printed Scaffolds for Bone Tissue Engineering. *Clin Rev Bone Miner Metab* 2015;13(4):245–255; doi: 10.1007/s12018-015-9198-5.
35. Letcher T. Material Property Testing of 3D-Printed Specimen in PLA on an Entry-Level 3D Printer. *Proc ASME 2014 Int Mech Eng Congr Expo* 2016;1–8.

36. Zhang B, Seong B, Nguyen VD, et al. 3D Printing of High-Resolution PLA-Based Structures by Hybrid Electrohydrodynamic and Fused Deposition Modeling Techniques. *J Micromechanics Microengineering* 2016;26(2); doi: 10.1088/0960-1317/26/2/025015.
37. Grémare A, Guduric V, Bareille R, et al. Characterization of Printed PLA Scaffolds for Bone Tissue Engineering. *J Biomed Mater Res - Part A* 2018;106(4):887–894; doi: 10.1002/jbm.a.36289.
38. Zhu W, Ma X, Gou M, et al. 3D Printing of Functional Biomaterials for Tissue Engineering. *Curr Opin Biotechnol* 2016;40:103–112; doi: 10.1016/j.copbio.2016.03.014.
39. Jacobs T, Declercq H, De Geyter N, et al. Plasma Surface Modification of Polylactic Acid to Promote Interaction with Fibroblasts. *J Mater Sci Mater Med* 2013;24(2):469–478; doi: 10.1007/s10856-012-4807-z.
40. Vunjak-Novakovic G, Obradovic B, Martin I, et al. Dynamic Cell Seeding of Polymer Scaffolds for Cartilage Tissue Engineering. *Biotechnol Prog* 1998;14(2):193–202; doi: 10.1021/bp970120j.
41. Tsai H-H, Yang K-C, Wu M-H, et al. The Effects of Different Dynamic Culture Systems on Cell Proliferation and Osteogenic Differentiation in Human Mesenchymal Stem Cells. *Int J Mol Sci* 2019;20(16):4024; doi: 10.3390/ijms20164024.
42. Kaspar D, Seidl W, Neidlinger-Wilke C, et al. Dynamic Cell Stretching Increases Human Osteoblast Proliferation and CICP Synthesis but Decreases Osteocalcin Synthesis and Alkaline Phosphatase Activity. *J Biomech* 2000;33(1):45–51; doi: 10.1016/S0021-9290(99)00171-2.
43. Kim MJ, Choi HJ, Cho J, et al. MG-63 Cell Proliferation with Static or Dynamic Compressive Stimulation on an Auxetic PLGA Scaffold. *Int J Polym Sci* 2017;2017; doi: 10.1155/2017/1286109.

Table 1: Parameters of the geometric modelling

	Diameter of Sphere Region	Mesh Size (mm)
Level 1	12	0.1
Level 2	24	0.5
Level 3	50	2.0
Level 4	100	10.0

Figure 1. The Illustration of the 3D Dynamic Cell Culture System Based on HPS. The 3D dynamic cell culture system consists of three main parts: 1. Hollow Porous Scaffold as a cell carrier provides the surface for cell adhesion and growth. 2. Tube with filter gap as a cell carrier and culture medium container. 3. Roller is the mechanical force resource to create the cell carrier's dynamic environment.

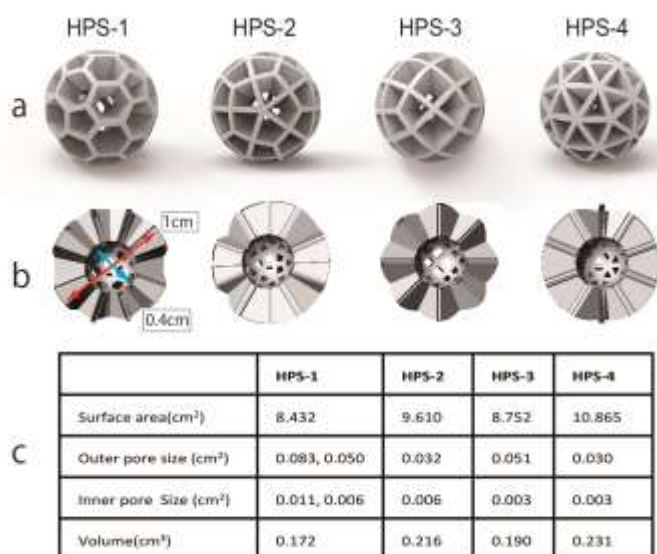


Figure 2. The schematic of HPS. (a) Four models of designed HPSs (diameter: 1 cm) with different outer porous structures. (b) All these models contain a similar inner hollow structure (diameter: 0.4 cm). (c) The parameters of surface area, pore size and volume of HPSs.

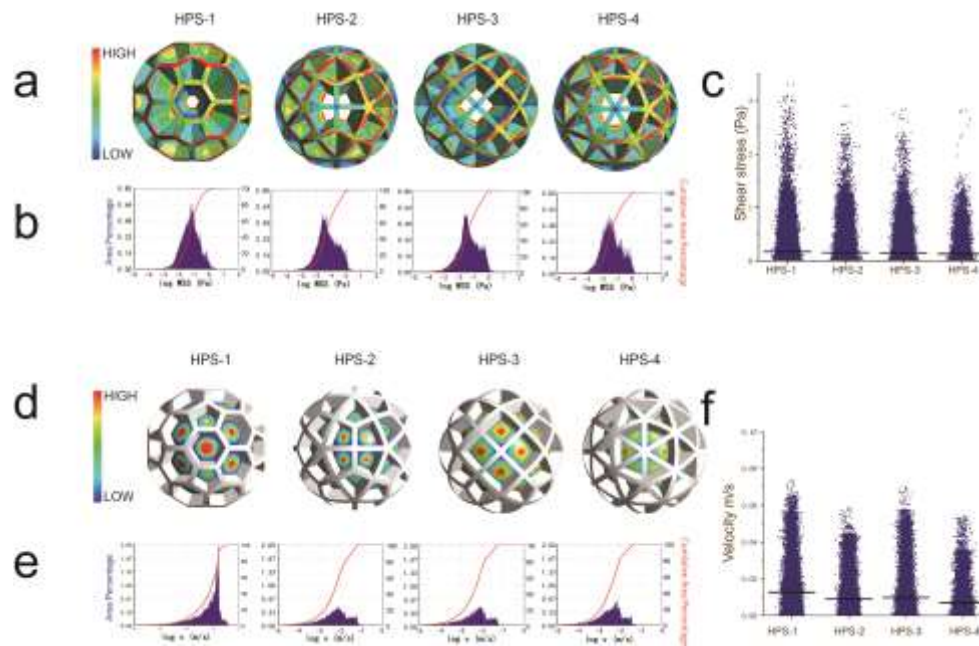


Figure 3. Surface shear stress and inside velocity of 4 HPSs in the fluid environment were analyzed *via* CFD simulation. (a) Colour contours of the magnitude of surface shear stress distributed at HPS models in the fluidity environment with inlet velocity at 0.1m/s. The colour bars indicated shear stress magnitude (pa). (b) Volumetric distribution of WSS (wall shear stress Pa, values in logarithm) of 4 HPSs. (c) The scatter plots graph of the surface shear stress of 4 HPSs. (d) Color contours of the inside velocity of HPSs in the fluidity environment with inlet velocity at 0.1m/s. Colour bars indicated velocity magnitude (m/s). (e) Volumetric distribution of velocity (m/s, values in logarithm) of 4 HPSs. (f) The scatter plot of the inside velocity of 4 HPSs.

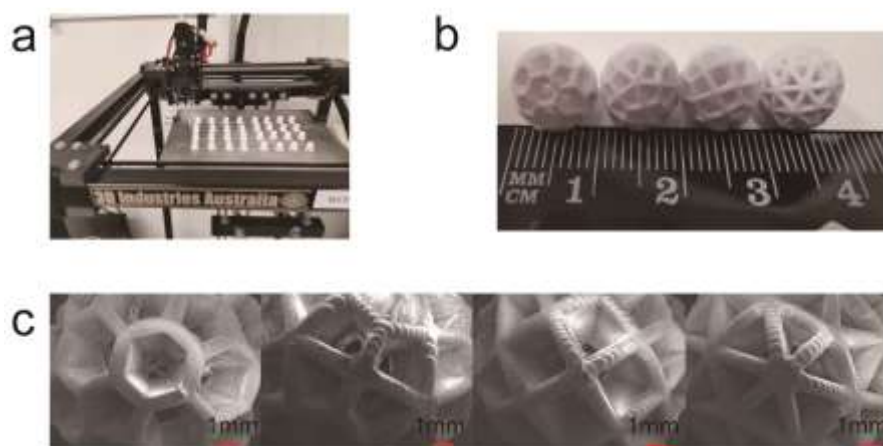


Figure 4. HPSs were fabricated by wombot 3D printer using PLA. (a) 32 HPSs were fabricated at one bath, which could satisfy the huge demand of further cell culture study. (b) Four HPSs (1cm diameter) were printed with structures consistent with designed geometries. (c) SEM images of the HPSs (scale bar =1mm).

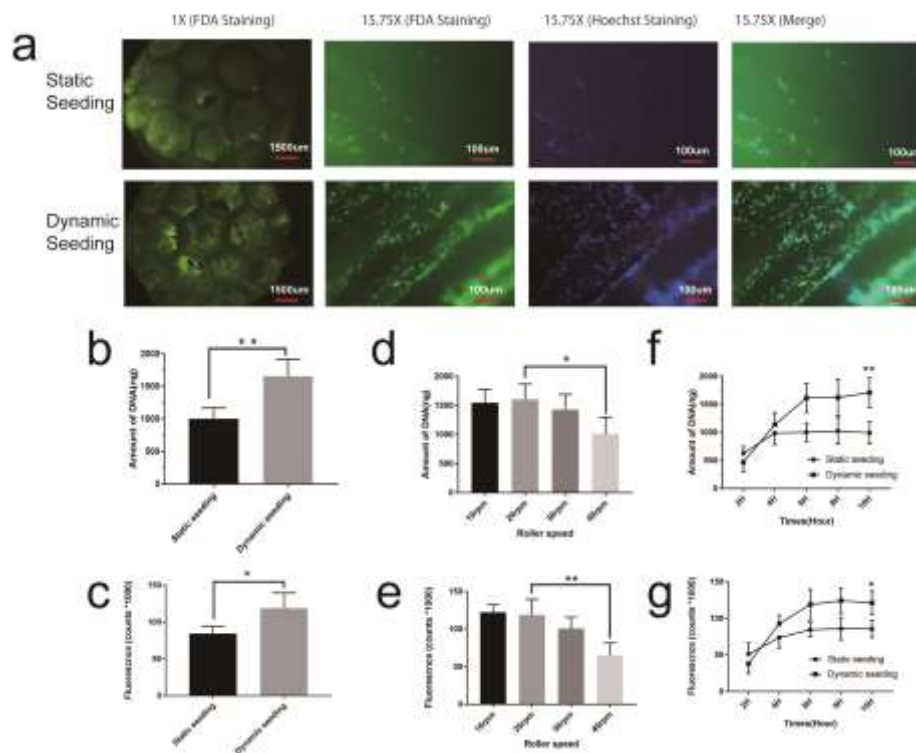


Figure 5. Cell seeding efficiency was compared between static and dynamic cell seeding methods. (a) FDA (green, for live cells) and Hoechst (blue, for cell nuclei) staining of cells on HPS after static and dynamic cell seeding. (b) PicoGreen assay test result showed the total DNA amounts of cells on HPS after static/dynamic cell seeding (** $p < 0.01$). (c) AlamarBlue assay result showed more cells growing on HPS after dynamic seeding, as compared to the static seeding ($*p < 0.05$). PicoGreen assay (d) and AlamarBlue assay results (e) showed high rotation speeds (over 20 rpm) and decreased cell adhesion on the HPS ($*p < 0.05$, $**p < 0.01$). PicoGreen assay (f) and AlamarBlue assay (g) results showed that 10 h were enough for the seeding procedure, and more cells adhered to the HPS after 10 h of dynamic seeding when compared to static seeding (** $p < 0.01$).

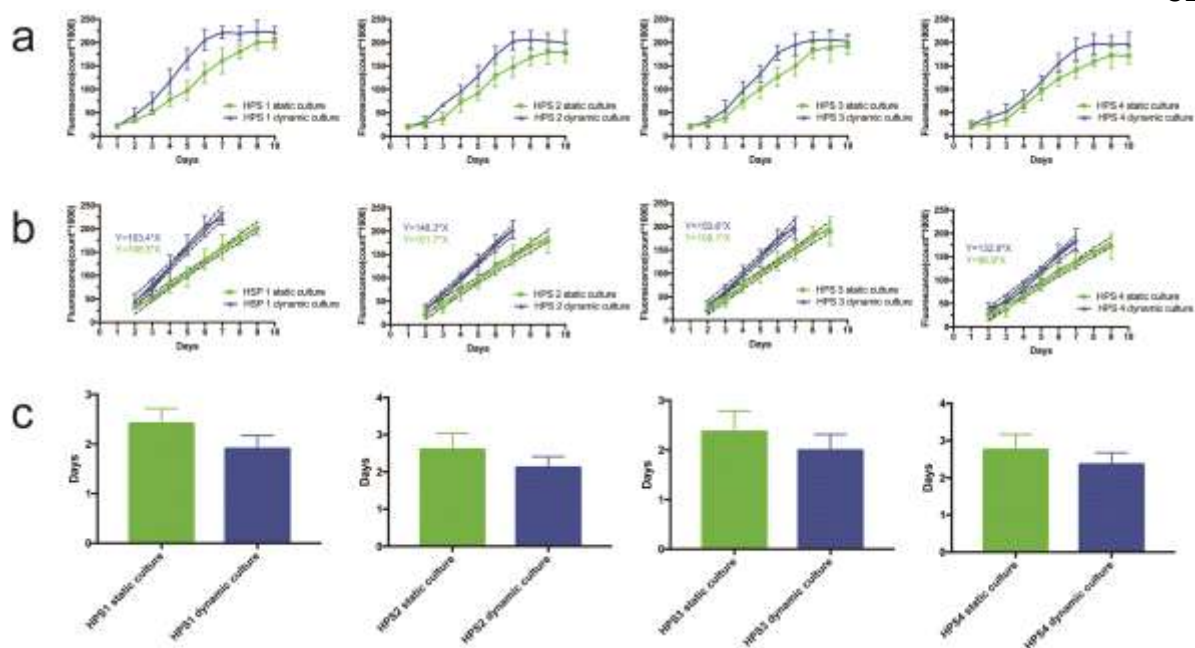


Figure 6. Effects of static and dynamic cell culture on cell proliferation in 4 different HPSs. (a) Growth curves of cells cultured on HPSs. Cell proliferation was assessed by alamarBlue assay after 10 days of static/dynamic cell culture, (b) Linear regression calculation was performed to assess cell proliferation speed based on alamarBlue assay results of the logarithmic phase cell growth. (c) Cell doubling time comparison of a static and dynamic culture.

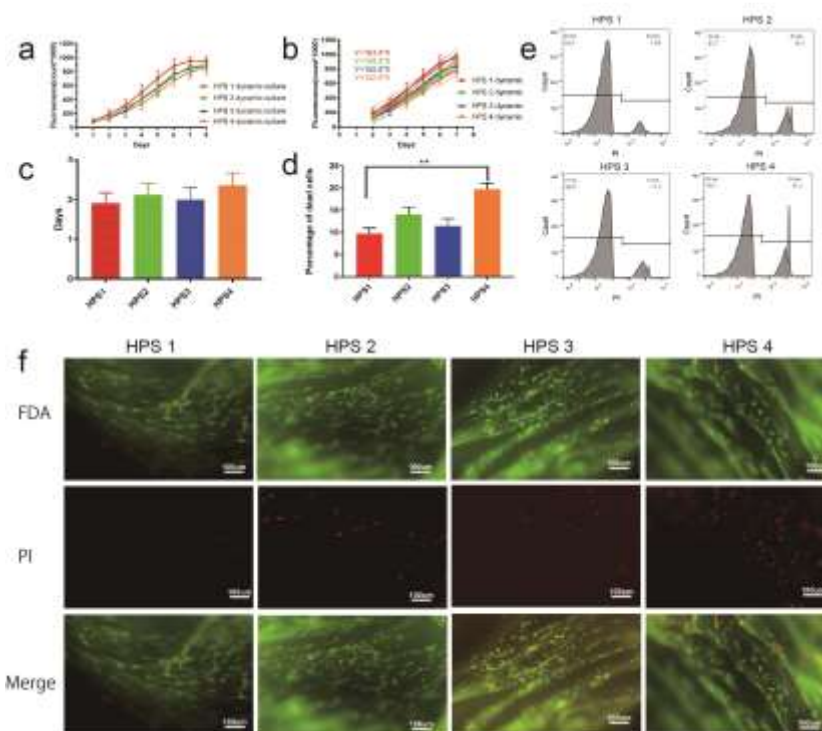


Figure 7. Cell proliferation profiles on 4 types of HPSs in a dynamic culture environment. (a) Cell proliferation was assessed by alamarBlue assay (roller speed: 10 rpm). (b) Linear regression calculation was performed to assess cell proliferation speed based on alamarBlue assay result of the logarithmic phase cell growth. (c) Comparison of cell doubling time on different HPSs. (d) Percentage of PI-positive cells on HPSs after 8 days of dynamic culture, (** $p < 0.01$). (e) Flow cytometry histogram of PI-stained cells on HPSs after 8 days of a dynamic culture. (f) FDA-PI double-staining images of cells on HPSs after 8 days of a dynamic culture.